Pharmaceutical Sciences and Drug Design
ISSN: 3062-4428
2025, Volume 5, Issue 2, Page No: 204-219

Available online at: www.galaxypub.co/page/journals

Galaxy Publication

Galaxy Publication

Isolation, Molecular Docking, and ADME Prediction of Bioactive Phytochemicals from *Pterocephalus frutescens* Targeting Cancer-Related Enzymes

Oliver Grant[1], David Clark[1]*, Sophia Nguyen[2]

[1]Department of Pharmaceutical Innovation and Drug Design, Faculty of Pharmacy, University of Glasgow, Glasgow, United Kingdom.
[2]Department of Molecular Therapeutics and Drug Discovery, Faculty of Pharmacy, National University of Singapore, Singapore.

***E-mail** ✉ david.clark@gmail.com

Received: 08 June 2026; **Revised:** 16 October 2026; **Accepted:**17 October 2026

ABSTRACT

In-silico modeling and computer-aided drug design benefit from the virtual evaluation of promising lead chemotherapeutic phytochemicals sourced from medicinal plants, which is accomplished by orienting and scoring ligands within a target protein's active binding cavity. The phytochemical exploration of a *Pterocephalus frutescens* n-butanol extract afforded the isolation and structural determination of three iridoids alongside four flavonoids, established respectively as Geniposide (1), Geniposidic acid (2), Nepetanudoside C (3), Isovitexin (4), Luteolin-7-O-glucoside (5), Isoorientin (6), and Orientin (7). The binding energies of these isolated phytochemicals were compared via molecular docking across four cancer-relevant biological receptors: aromatase, carbonic anhydrase IX, fatty acid synthase, and the topoisomerase II-DNA complex. Findings from the docking work revealed that the purified compounds harbor encouraging cytotoxic capabilities, especially Luteolin-7-O-glucoside (5) and Orientin (7), which registered remarkable binding affinities within the panel of isolates at the active pockets of the target proteins; Aromatase (−8.73 Kcal/mol), and Carbonic anhydrase IX (−8.92 Kcal/mol), correspondingly, outperforming the documented binding scores of both co-crystallized ligands and standard drugs at these enzymatic targets. Additionally, within the set of separated constituents, Luteolin-7-O-glucoside (5) exhibited the strongest binding interactions at the active sites of Fatty acid synthase and the Topoisomerase II-DNA complex, yielding binding values of −6.82 and −7.99 Kcal/mol, respectively. In the end, predictions from the SwissADME online portal indicated that most of these phytomolecules have satisfactory oral bioavailability and drug-likeness.

Keywords: Drug likeness, Lipinski's rule, Molecular docking, *Pterocephalus frutescens*, Chemical profiling, Phytochemicals

How to Cite This Article: Grant O, Clark D, Nguyen S. Isolation, Molecular Docking, and ADME Prediction of Bioactive Phytochemicals from *Pterocephalus frutescens* Targeting Cancer-Related Enzymes. Pharm Sci Drug Des. 2025;5(2):204-19. https://doi.org/10.51847/Z0YeBVmMNx

Introduction

Encompassing 42 genera and roughly 860 species, the Caprifoliaceae family is primarily distributed in Europe, Asia, and Africa, with some representatives introduced and successfully established in other territories [1]. The genus Pterocephalus contains 25 species, known worldwide for their antimicrobial, anti-inflammatory, free radical-scavenging, liver-protective, and pain-relieving effects [2-5]. A range of natural products underlying these biological actions in the Pterocephalus genus have been purified, including flavonoids, iridoids, phenolic acids, saponins, and lignans [6-9]. In the clinical realm, chemotherapy is a cornerstone modality in cancer management; therefore, the discovery of actionable chemotherapeutic targets remains an active area of investigation [10, 11]. The use of plant-derived molecules in oncological therapy is widely described in the scientific literature. Vincristine and paclitaxel are prominent examples of phytochemicals used in clinical chemotherapy protocols

[12]. Flavonoids constitute another phytochemical class with considerable chemotherapeutic and cancer-preventative promise, as well as recognized anti-inflammatory properties [13, 14].

Numerous biomolecular entities have been probed as targets for the tailored treatment of various cancer forms. This therapeutic paradigm focuses on identifying individual proteins implicated in neoplastic growth and division, enabling chemotherapeutic agents to impede cancer dissemination. Among the identified biological targets, aromatase, carbonic anhydrase IX, fatty acid synthase, and the topoisomerase II-DNA complex have drawn considerable focus. Aromatase is a pivotal enzyme in estrogen biosynthesis, orchestrating androgen aromatization; estrogens are established as key drivers of mammary carcinogenesis [15]. Multi-targeted chemotherapeutic approaches have also recently involved aromatase [16, 17]. Certain phytochemical entities, exemplified by the flavonoids rotenone, chrysin, and apigenin, have demonstrated potent suppression of the aromatase cytochrome p450 enzyme [18].

Regarding fatty acid synthase (FAS), this enzyme is the principal catalyst for the synthesis of diverse fatty acids and is abundantly overexpressed in numerous neoplastic conditions [19]. Consequently, it confers metabolic adaptability, especially in tumors with a lipogenic phenotype [20]. This metabolic role has positioned FAS as an alluring drug target, where particular flavonoid phytochemicals were shown to mediate a dose-dependent link between FAS suppression and the triggering of programmed cell death in malignant cells [21].

Another critical category encompasses the topoisomerase enzymes, which perform essential catalytic functions in modulating the three-dimensional architecture of DNA. Human topoisomerases are classified into two types (I and II), with the Topoisomerase II variant (ATP-binding region) facilitating double-stranded DNA cleavage [22]. These enzymes have been extensively studied as targets for both antimicrobial and anticancer agents [23]. A recent study by Han *et al*. [24] reinforced the therapeutic value of topoisomerase inhibitors in cancer treatment, while highlighting off-target toxicity as the principal limiting factor. Exploration of naturally sourced phytochemicals—including podophyllotoxin, anthracyclines, genistein, and camptothecin—has focused on suppressing topoisomerase I and II in various tumor models [25, 26]. An additional central contributor to neoplastic advancement is carbonic anhydrase IX (CAIX), whose expression is triggered by intratumoral hypoxia and the resulting acidic milieu. This enzyme equips mutated cells to survive the hostile microenvironment generated by their mutations, thereby granting them a selective advantage for propagation and disease progression [27]. Accordingly, numerous investigations have assessed CAIX inhibition as a strategy for tumor management [28, 29].

The investigation described herein sought to delineate the principal phytochemical composition of *Pterocephalus frutescens* raw material using isolation and structural identification techniques. A complementary in silico analysis of the obtained phytochemicals was conducted to assess their potential chemotherapeutic relevance, employing molecular docking to probe their binding potential against cancer-related molecular targets: aromatase, carbonic anhydrase IX, fatty acid synthase, and the topoisomerase II-DNA complex. To further assess the promise of these candidates from a drug metabolism and pharmacokinetics standpoint, the SwissADME web-based platform, developed by the molecular modeling division of the Swiss Institute of Bioinformatics (SIB), was used to compute their physicochemical descriptors and predict their pharmacokinetic behavior and drug-likeness [30].

Materials and Methods

Plant material

Specimens of *P. frutescens* Hochst. Aerial tissues were harvested at the flowering stage in June 2017 from Jabal An-NabiShu'ahyb, Sanaa, within the Republic of Yemen. Botanical collection, taxonomic determination, and authentication were performed by Dr. Abdo H. Marey, Professor of Botany and Plant Taxonomy, Faculty of Science, Al-Azhar University, Cairo, Egypt. A reference voucher specimen was archived at the Herbarium of the Faculty of Pharmacy, Al-Azhar University, Cairo, Egypt.

Extraction and isolation of pure compounds

Shade-dried, finely comminuted aerial biomass of *P. frutescens* (250 g) was subjected to sequential Soxhlet extraction employing n-hexane (2 × 2 L) first, then methanol (3 × 3 L), which, after concentration under reduced pressure via rotary evaporator (BUCHI Rotavapor® R-210/R-215, Labfirst Scientific, CA, USA), furnished 7.5 and 35 g of residue, respectively. A 35 g aliquot of the methanol-soluble material was taken up in water and underwent consecutive liquid–liquid partitioning against ethyl acetate (2 × 200 mL) and water-presaturated n-

butanol (3 × 200 mL), delivering light brown dried masses of 8.5 and 11 g, in that order. The n-butanol-soluble portion (11 g) was fractionated on a polyamide stationary phase (200 g) using step-gradient elution from water: methanol (100:0) to (0:100), yielding four pooled fractions. Fraction 2 (1.8 g) was reloaded onto a silica gel column (40 g) and eluted with a chloroform:methanol:water gradient (90:10:1), resolving into three sub-fractions. Sub-fraction 2 (360 mg) was further refined on a silica gel bed, employing sequential elution with chloroform: methanol (90:10) and (85:15) to yield five sub-fractions. Sub-fractions 2.1, 2.4, and 2.5 (weighing 50, 60, and 40 mg, respectively) were each independently polished on a Sephadex LH20 column (50 g) running methanol, ultimately isolating compounds (1), (2), and (3) (22, 38, and 30 mg, respectively). Fraction 3 (2.3 g) was re-subjected to silica gel chromatography (80 g) under isocratic conditions with benzene:methanol:water (100:50:3), giving rise to five sub-fractions. Sub-fraction 3.5 (500 mg) was further chromatographed through Sephadex LH20 (100 g) eluting with methanol to obtain compound (4) (25 mg). Fraction 4 (1.9 g) was processed on a reversed-phase (RP) solid-phase extraction (SPE) cartridge (50 g) using a water: methanol gradient (90:10–10:90), which yielded four subfractions. Purification of sub-fraction 4.1 (280 mg) over Sephadex LH20 (100 g) with isocratic methanol yielded compound (5) (15 mg). Sub-fractions 4.2 (200 mg) and 4.3 (340 mg) were separately polished on Sephadex LH20 (100 g) eluting isocratically with methanol: chloroform (60:40), providing compound (6) (14 mg) and compound (7) (32 mg).

Structure elucidation of isolated pure compounds

Nuclear magnetic resonance (NMR) data were collected on a Bruker spectrometer (Rheinstetten, Karlsruhe, Germany). Deuterated methanol (CD3OD) and dimethyl sulfoxide (DMSO-d6) were employed as solvents for spectral acquisition.

Molecular docking analysis

A molecular docking investigation was carried out to probe the anticancer attributes of the yielded compounds versus four pertinent biological receptors, specifically, aromatase enzyme, carbonic anhydrase IV, fatty acid synthase, and topoisomerase II-DNA complex, deploying the Autodock software suite.

Preparation of the investigated compounds

The chemical architectures of the phytochemicals under study were constructed in ChemBioDraw Ultra 14.0 **(Figure 1)** to prepare them for docking simulations, as outlined in earlier reports [31-38]. For every macromolecular target, the furnished compounds were assembled into a unified database and stored using an MDB file format.

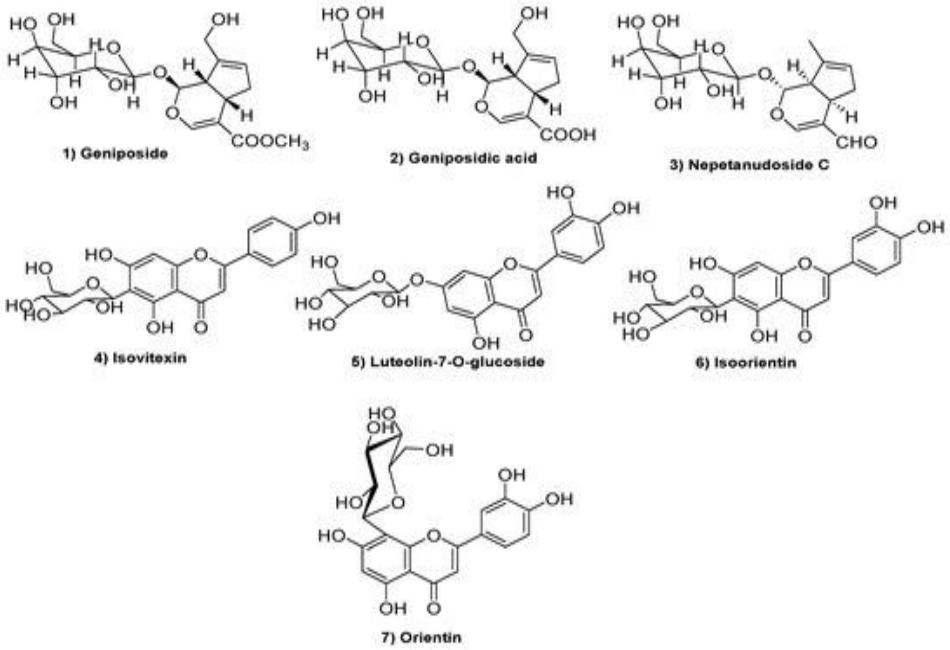

Figure 1. Chemical structures of the flavonoid and iridoid constituents isolated from *P. frutescens* Hochst.

Preparation of the target proteins

Crystallographic coordinates for the selected biological targets were retrieved from the Protein Data Bank. The assigned PDB identifiers for the aromatase enzymes CA IV, FAS, and TOP II were 5jl9 [39], 5fl4 [40], 2px6 [41], and 3qx3 [42], respectively. The protein structures were subsequently prepared by adding hydrogen atoms, mending any disrupted bonds, and performing energy minimization to ready them for the downstream docking protocol, following previously documented procedures in full detail [31].

Results and Discussion

Structural elucidation of isolated pure compounds

Compound (1) was obtained as white crystals with ESIMS m/z: 387 $[M-H]^-$; (calculated for $C_{17}H_{24}O_{10}$)**.** ^{1}H NMR (CD_3OD, 400 MHz) δ 5.19 (1H, d, J = 7.5 Hz, H-1) 7.53 (1H, s, H-3); 3.22 (1H, overlap, H-5); 2.13 (1H, m, H-6a); 2.84 (1H, dd, J = 8.0, 16.0Hz, H-6b); 5.82 (1H, s, H-7); 2.74 (1H, t, J = 7.5 Hz, H-9); 4.20 (1H, d, J = 14.5 Hz, H-10a); 4.33 (1H, d, J = 14.5 Hz, H-10b); 3.73 (3H, s, H-12); 4.73 (1H, d, J = 7.5 Hz, H-1'); 3.23–3.41 (4H, m, H-2′, 3′, 4′, 5′); 3.65 (1H, dd, J = 4.0, 9.5 Hz, H-6a′); 3.88 (1H, brd, J = 12.0 Hz, H-6b′). ^{13}C-NMR (CD_3OD, 100 MHz) δ 100.2 (C-1); 155.3 (C-3); 114.5 (C-4); 38.6 (C-5); 41.8 (C-6); 130.3 (C-7); 146.9 (C-8); 49.1 (C-9); 63.5 (C-10); 171.6 (C-11); 53.8 (C-12); 102.4 (C-1′); 76.9 (C-2′); 80.0 (C-3′); 73.7 (C-4′); 80.6 (C-5′); 63.7 (C-6′). From the above data, compound (**1**) was identified as Geniposide [43].

Compound (2) was obtained as an amorphous powder with ESIMS m\z: 363 $[M-H]^-$; (calculated for $C_{16}H_{22}O_{10}$). ^{1}H NMR (CD_3OD, 400 MHz) δ 5.11 (1H, d, J = 7.5 Hz, H-1), 7.31 (1H, s, H-3), 3.23 (1H, m,H-5), 2.09 (1H, dd, J = 16.2/7.6 Hz, Ha-6), 2.86 (1H, dd, J = 16.2/7.6 Hz, Hb-6), 5.79 (1H, brs, H-7), 2.70(1H, t, J = 7.5 Hz, H-9), 4.18 (1H, d, J = 14.6 Hz, Ha-10), 4.33 (1H, d, J = 14.3 Hz, Hb-10), 4.74 (1H, d, J= 7.6 Hz, H-1′), 3.18–3.45 (4H, m, H-2′, H-3′, H-4′, H-5′), 3.69 (1H, dd, J = 11.9/5.5 Hz, Ha-6′), 3.85 (1H, dd, J = 11.6/1.7 Hz, Hb-6′). ^{13}C-NMR (CD_3OD, 100 MHz) δ 98.2 (C-1), 153.2 (C-3), 112.8 (C-4), 36.7 (C-5), 39.7 (C-6), 127.8 (C-7), 143.3 (C-8), 47.0 (C-9), 61.4 (C-10), 173.0 (C-11), 100.3 (C-1), 74.8 (C-2), 77.4 (C-3), 71.5 (C-4), 78.8 (C-5), 62.6 (C-6). From the above data, compound (**2**) was identified as Geniposidic acid [43].

Compound (3) was obtained as an amorphous powder with ESIMS m\z: 341 $[M-H]^-$; (calculated for $C_{16}H_{22}O_8$). ^{1}H NMR (CD_3OD, 400 MHz) δ 5.40 (d, 4.6, H-1), 7.34 (s, H-3), 3.13 (m, H-5), 2.18 (m, H-6), 2.76 (m, H-6), 5.49 (m, H-7), 2. 91(m, H-9), 1.82 (br s, H3-10), 9.21 (s, H-11), 4.64(d, 7.6, H-1′), 3.69 (dd, 12.0, 3.8, H-6a′), 3.87 (br d, 12.0, H-6b′); 3.22–3.42 (4H, m, H-2′, H-3′, H-4′, H-5′). ^{13}C-NMR (CD_3OD, 100 MHz) δ 101.4 (C-1), 158.8 (C-3), 121.6 (C-4), 32.8 (C-5), 38.5 (C-6), 128.2 (C-7), 139.5 (C-8), 50.45 (C-9), 15.3 (C-10), 193.4 (C-11), 103.8 (C-1), 75.5 (C-2), 78.7 (C-3), 71.5 (C-4), 78.4 (C-5), 62.2 (C-6). From the above data, compound (**3**) was identified as Nepetanudoside C [44].

Compound (4) was obtained as a yellow powder with ESIMS m\z: 431 $[M-H]^-$; (calculated for $C_{21}H_{20}O_{10}$). ^{1}H NMR (DMSO-d_6, 400 MHz) δ 13.48 (1H, brs, 5-OH), 7.79 (2H, d, J = 8.3 Hz, 3′, 5′-H), 6.89 (2H, d, J = 8.2 Hz, 2′, 6′-H), 6.70(1H, s, 3-H), 6.39 (1H, s, 8-H), 4.51 (1H, d, J = 9.7 Hz, 1″-H). 3.40–3.95 (sugar protons, m). ^{13}C-NMR (DMSO-d_6, 100 MHz) δ 163.71 (C-2), 102.90(C-3), 181.83 (C-4), 160.52 (C-5), 108.82 (C-6), 163.55 (C-7), 93.94 (C-8), 155.91 (C-9), 102.76 (C-10), 121.24 (C-1'), 128.65 (C-2', 6'), 115.89 (C-3', 5'), 161.46 (C-4'), 73.55 (C-1″), 70.86 (C-2″)), 79.03 (C-3″)), 70.43 (C-4″), 81.53 (C-5″), 61.42 (C-6″). From the above data, compound (**4**) was identified as Isovitexin [45].

Compound (5) was obtained as a yellow crystalline powder, with ESIMS m\z: 447 $[M-H]^-$; (calculated for $C_{21}H_{20}O_{11}$). ^{1}H NMR (DMSO-d_6, 400 MHz) 13.13 (1H, s, 5-OH), 7.49 (1H, dd, J = 2.2, 8.2 Hz, H-6′), 7.43 (1H, d, J = 2.2 Hz, H-2′), 6.91 (1H, d, J = 8.2 Hz, H-5′), 6.68 (1H, s, H-3), 6.32(1H, s, H-6), 4.67 (1H, d, J = 9.3 Hz, H-1″), 3.30–3.90 (sugar protons, m). ^{13}C-NMR (DMSO-d_6, 100 MHz) δ 164.32(C-2), 102.75 (C-3), 182.32 (C-4), 160.76 (C-5), 98.32 (C-6), 162.96 (C-7), 105.05 (C-8), 156.60 (C-9), 104.30(C-10), 122.11 (C-1′), 114.57 (C-2′), 146.15 (C-3′), 150.20 (C-4′), 115.88 (C-5′), 119.64 (C-6′), 73.67 (C-1″),70.99 (C-2″), 78.97 (C-3″), 70.93 (C-4″), 82.20 (C-5″), 61.96 (C-6″). From the above data, compound (**5**) was identified as Orientin [46].

Compound (6) was obtained as a yellow powder, with ESIMS m\z: 447 $[M-H]^-$; (calculated for $C_{21}H_{20}O_{11}$). ^{1}H NMR (DMSO-d_6, 400 MHz) δ 13.53 (1H, brs, 5-OH), 7.42 (1H, dd, J = 2.4 Hz, 9.0 Hz, 6′-H), 7.36 (1H, d, J = 2.4 Hz, 2′-H), 6.90 (1H, d, J = 9.0 Hz, 5′-H), 6.64 (1H, S, 3-H), 6.48(1H, s, H-8), 4.58 (1H, d, J = 10.0 Hz, 1″-H). 3.30–3.90 (sugar protons, m). ^{13}C-NMR (DMSO-d_6, 100 MHz) δ 163.65 (C-2), 102.76 (C-3), 181.86 (C-4), 160.91 (C-5), 108.95 (C-6), 163.78 (C-7), 94.04 (C-8), 156.75 (C-9), 102.91 (C-10), 121.86 (C-1'), 113.32 (C-2'), 146.34

(C-3'), 150.73 (C-4'), 116.53 (C-5'), 119.21 (C-6'), 73.42 (C-1″)),70.53 (C-2″)), 79.23 (C-3″), 70.43 (C-4″), 81.78 (C-5″), 61.68 (C-6″). From the above data, compound (**6**) was identified as Isoorientin [46].

Compound (7) was obtained as a yellow microcrystalline powder with ESIMS m\z: 447 $[M-H]^-$; (calculated for $C_{21}H_{20}O_{11}$). ^{1}H NMR (DMSO-d_6, 400 MHz) δ 6.54 (1H, d, J = 1.5 Hz, H-6), 6.84 (1H, s,H-3), 6.87 (1H, d, J = 1.5 Hz, H-8), 6.85 (1H, d, J =8.1 Hz, H-5′), 7.55 (2H, d, J = 8 Hz, H-2′,6′). 5.01 (1H, d, J = 7.5 Hz, H-1″), 4.36 (1H, d, J_12.8 Hz, H-6″a), 4.15 (2H, m, H-3″, H-6″b), 4.08 (1H, m, H-2″), 4.02 (2H, m, H-4″, H-5″). ^{13}C-NMR (DMSO-d_6, 100 MHz) δ 61.65 (C-6″), 70.76 (C-4″), 73.92 (C-2″), 77.35 (C-3″), 78.00 (C-5″),95.76 (C-8), 100.36 (C-6), 100.87 (C-1″), 103.95(C-3), 106.43 (C-10), 114.43 (C-2′), 116.84 (C-5′),119.98 (C-6′), 121.89 (C-1′), 146.74 (C-3′), 151.53(C-4′), 157.74 (C-9), 162.05 (C-5), 163.90 (C-2),165.53 (C-7), 182.84 (C-4). From the above data, compound (**7**) was identified as Luteolin-7-O-glucoside (cynaroside) [47].

Results of in silico studies

Molecular docking analysis

The molecular docking experiments were performed to assess how strongly Geniposide (1), Geniposidic acid (2), Nepetanudoside C (3), Isovitexin (4), Luteolin-7-O-glucoside (5), Isoorientin (6), and Orientin (7) could bind to the selected biological macromolecules, namely aromatase, carbonic anhydrase IX, fatty acid synthase, and the topoisomerase II-DNA complex. An initial validation step was undertaken to confirm the precision of the AutoDock software used in the study. This validation entailed repositioning the native co-crystallized ligand back into its corresponding target structure. The process yielded reassuringly low RMSD measurements (1.84, 1.72, 1.88, and 1.42 Å for aromatase, carbonic anhydrase IX, fatty acid synthase, and the topoisomerase II-DNA complex, respectively), thereby verifying the program's reliability [32, 48-52]. With validation confirmed, docking was used to gain a deeper understanding of the binding characteristics of the isolated compounds within these protein targets, helping elucidate their potential as promising new anticancer agents. The calculated binding free energies, RMSD values, and the specific intermolecular interactions for the docked compounds are summarized in **Tables 1 and 2**.

Table 1. Binding scores, RMSD values, and amino acid binding interactions of the investigated compounds against aromatase and carbonic anhydrase IX.

Aromatase enzyme				
Comp. No	**RMSD (Å)**	**S score (Kcal/mol)**	**Binding interactions**	**Distances (Å)**
(1)	0.70	−8.15	LEU372 (H-donor)MET374 (H-acceptor)	2.933.10
(2)	0.89	−7.70	CYS437 (H-donor)MET374 (H-donor)LEU477 (H-donor)	3.304.503.26
(3)	1.49	−7.22	LEU372 (H-donor)LEU477 (H-donor)MET374 (H-acceptor)ALA306 (H-acceptor)	3.122.943.193.38
(4)	2.27	−8.54	LEU477 (H-donor)LEU477 (H-donor)MET374 (H-acceptor)ILE133 (π-H)	2.832.723.374.22
(5)	1.74	−8.73	MET374 (H-donor)LEU372 (H-donor)LEU477 (H-donor)ILE133 (π-H)	3.842.713.254.49
(6)	1.27	−8.52	MET303 (H-donor)MET303 (H-donor)LEU477 (H-donor)LEU477 (H-donor)MET374 (H-acceptor)ILE133 (π-H)GLY439 (π-H)	4.243.913.102.663.033.964.36
(7)	1.81	−8.67	MET374 (H-donor)MET374 (H-acceptor)	3.923.03
Co-crystallized	1.84	−8.02	MET374 (H-acceptor)	2.97
Reference	1.07	−7.76	MET374 (H-acceptor)	2.96
CA IX				

Comp. No	RMSD (Å)	S score (Kcal/mol)	Binding interactions	Distances (Å)
(1)	1.43	−7.41	GLU106 (H-donor)THR200 (H-acceptor)	3.143.07
(2)	1.45	−7.05	THR201 (H-donor)THR200 (H-acceptor)	2.673.23
(3)	1.64	−7.41	THR201 (H-donor)THR200 (H-acceptor)HIS94 (π-H)	2.883.173.55
(4)	1.41	−7.21	THR201 (H-donor)GLN71 (H-acceptor)ZN264 (Metal)LEU91 (π-H)GLN92 (π-H)	3.183.032.303.983.85
(5)	1.83	−8.13	GLU106 (H-donor)	3.08
(6)	1.31	−7.41	ZN264 (Metal)	2.30
(7)	2.13	−8.92	THR201 (H-donor)	3.22
Co-crystallized	1.72	−5.91	THR201 (H-donor)THR200 (H-acceptor)VAL121 (π-H)	3.273.344.93
Reference	1.31	−5.83	THR201 (H-donor)THR201 (H-donor)THR200 (H-acceptor)	3.293.223.28

Table 2. Binding scores, RMSD values, and amino acid binding interactions of the investigated compounds against FAS and topoisomerase II-DNA complex.

FAS				
Comp. No	**RMSD**	**S score**	**Binding interactions**	**Distances**
(1)	0.93	−5.86	SER2340 (H-acceptor)ARG2482 (H-acceptor)	3.123.23
(2)	1.84	−6.05	ASP2338 (H-donor)PRO2341 (H-donor)SER2340 (H-acceptor)TYR2462 (π-H)	3.012.913.193.54
(3)	0.93	−5.85	SER2308 (H-donor)THR2342 (H-donor)SER2340 (H-acceptor)HIS2481 (π-H)	2.953.233.073.73
(4)	1.09	−6.22	THR2342 (H-donor)SER2340 (H-acceptor)	3.053.35
(5)	2.26	−6.82	SER2340 (H-donor)SER2340 (H-acceptor)PHE2370 (π-H)ILE2250 (π-H)	2.973.024.533.80
(6)	1.10	−6.49	SER2340 (H-donor)	3.00
(7)	1.61	−6.40	HIS2481 (H-donor)	3.33
Co-crystallized	1.39	−8.09	SER2340 (H-acceptor)TYR2462 (π-H)HIS2481 (π-H)	3.034.654.42
Reference	1.76	−6.03	HIS2481 (π–π)	3.92
Topoisomerase II–DNA Complex				
Comp. No	**RMSD**	**S score**	**Binding interactions**	**Distances**
(1)	1.77	−7.31	DG10 (H-donor)ASP479 (H-donor)DT9 (π-H)	2.962.863.78
(2)	1.46	−6.87	MET782 (H-donor)ARG503 (H-acceptor)	3.162.99
(3)	1.44	−7.16	ARG503 (H-acceptor)ASP479 (H-acceptor)DG13 (π-H)DG13 (π-H)	3.012.954.543.68
(4)	1.15	−7.47	ASP479 (H-donor)DT9 (π-H)DT9 (π-H)	3.084.164.21
(5)	2.15	−7.99	ASP479 (H-donor)DG10 (H-donor)SER480 (H-acceptor)DT9 (π-H)	2.693.202.923.64
(6)	1.49	−7.78	ASP479 (H-donor)DT9 (H-donor)	2.982.97
(7)	2.18	−7.69	ASP479 (H-donor)DT9 (H-donor)GLU477 (H-donor)ARG503 (H-acceptor)DG13 (π-H)DT9 (π-H)	3.002.713.033.113.664.47

Co-crystallized	1.42	−10.52	ASP479 (H-donor)MET782 (H-donor)DG13 (H-donor)GLN778 (H-acceptor)DA12 (π-H)	2.703.733.372.943.75
Reference	1.84	−8.96	ARG503 (H-donor)ASP479 (H-acceptor)LYS456 (H-acceptor)DG13 (π-H)	3.243.433.294.26

Examining the docking data for the aromatase target, a notable observation was that compounds (4, 5, 6, and 7) achieved favorable binding scores that outperformed those recorded for both the co-crystallized ligand and the comparator drug (Exemestane). The rationale for selecting exemestane as a benchmark was its function as an aromatase inhibitor, alongside its polycyclic architecture, which resembles the structures of the test compounds; this structural similarity supports a reliable assessment that the compounds can securely anchor within the target's active site for a valid comparative analysis. It is worth noting that compound (5) showed the highest binding affinity for the aromatase enzyme among the entire set. Furthermore, the amino acid MET374 appears to be a crucial residue for aromatase inhibition, as it interacts with both the co-crystallized ligand and the reference drug. The results showed that compound (5) engages the aromatase enzyme with a binding energy of −8.73 Kcal/mol and an RMSD of 1.74 Å. Specifically, hydrogen bonds were formed by the glycosidic component of compound (5) with the residues MET374, LEU372, and LEU477 at separations of 3.84, 2.71, and 3.25 Å, respectively. A pi-H interaction was also established between the phenyl ring of compound (5) and ILE133 at a distance of 4.49 Å. By contrast, the co-crystallized ligand contributed a single hydrogen bond to MET374 (2.97 Å), and the reference inhibitor (Exemestane) similarly formed a hydrogen bond with MET374 at a distance of 2.96 Å, as shown in **Figure 2.**

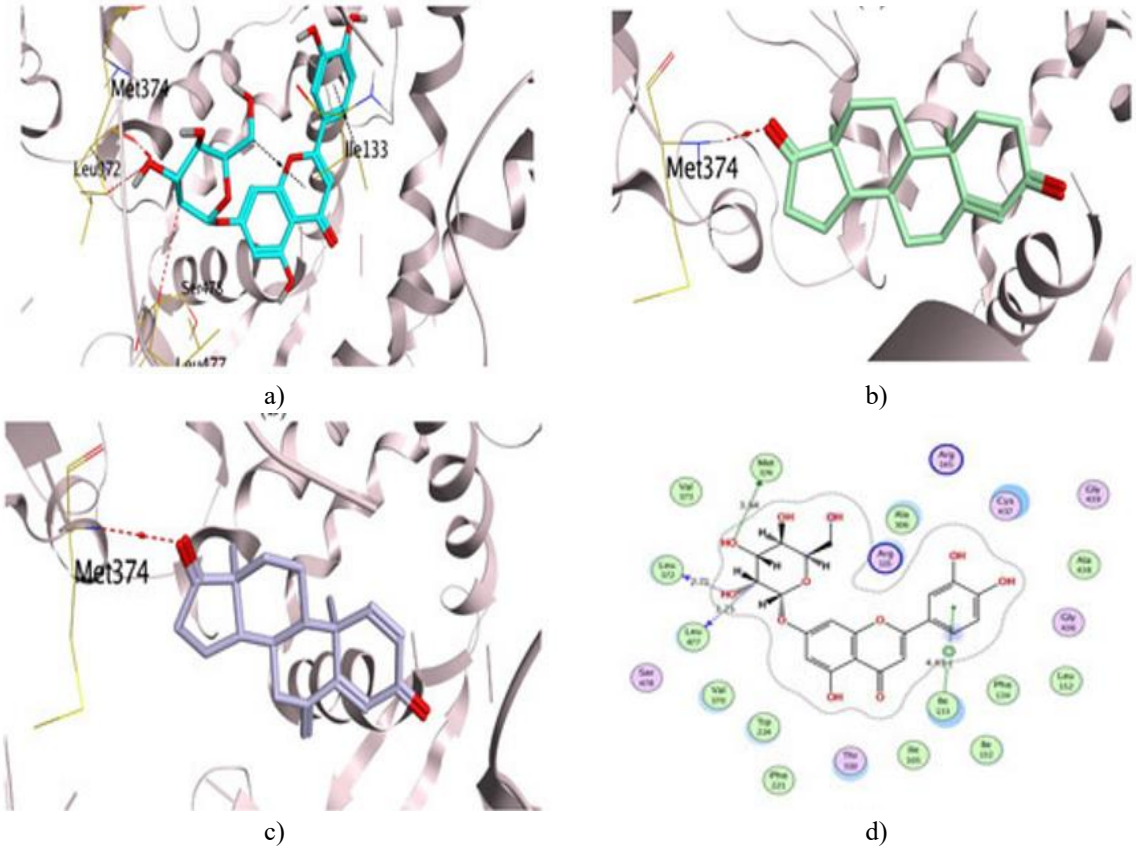

a) b) c) d)

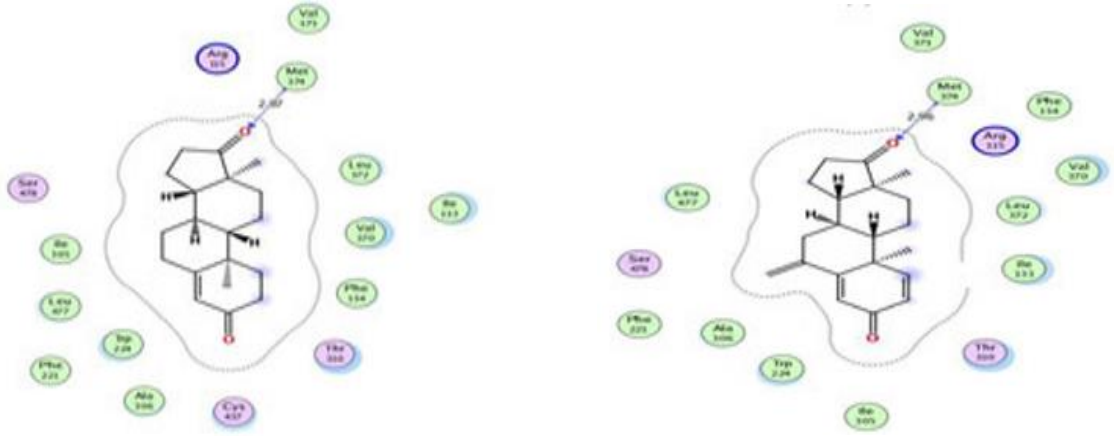

e) f)

Figure 2. The 3D binding interactions of (a) compound (5), (b) the co-crystallized ligand, (c) the reference drug, and the 2D binding interactions of (D) compound (5), (e) the co-crystallized ligand, and (f) the reference drug at the aromatase enzyme.

Shifting focus to the carbonic anhydrase IX (CA IX) target, a striking finding was that compound (7) possessed the greatest binding potential for CA IX relative to the other compounds. The residues THR200 and THR201 were inferred to be essential for inhibiting CA IX, as they are engaged by both the co-crystallized ligand and the reference drug. The data disclosed that compound (7) binds to CA IX with a score of −8.92 Kcal/mol and an RMSD value of 2.13 Å. A key interaction involved a hydroxyl substituent on the sugar unit of compound (7), which formed a hydrogen bond to THR201 at 3.22 Å. In the case of the co-crystallized ligand, its sulfamoyl group was responsible for hydrogen-bonding contacts with THR200 (3.34 Å) and THR201 (3.27 Å), and its thiophene moiety participated in a pi-H contact with VAL121 at a distance of 4.93 Å. Meanwhile, the reference compound (Acetazolamide) formed a hydrogen bond with THR200 via its sulfamoyl group (3.28 Å) and two additional hydrogen bonds with THR201 through its thiadiazole ring and amide portion at 3.22 and 3.29 Å, respectively, as illustrated in **Figure 3**.

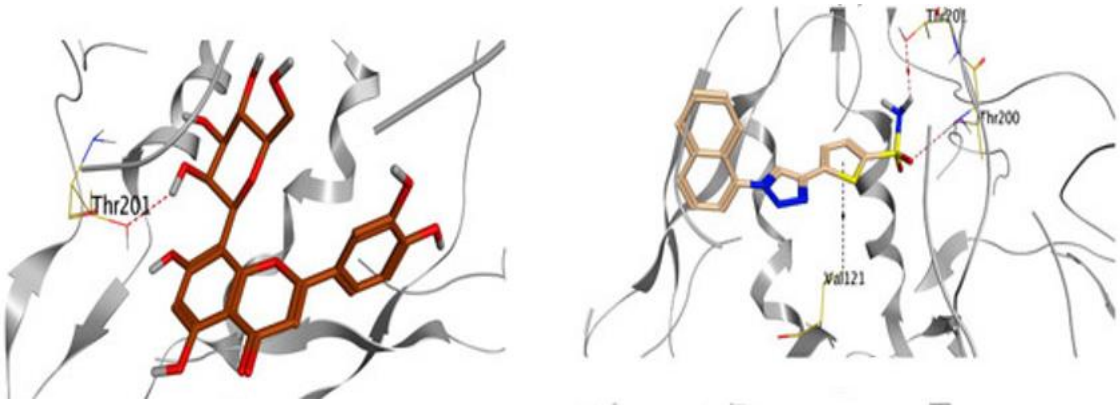

a) b)

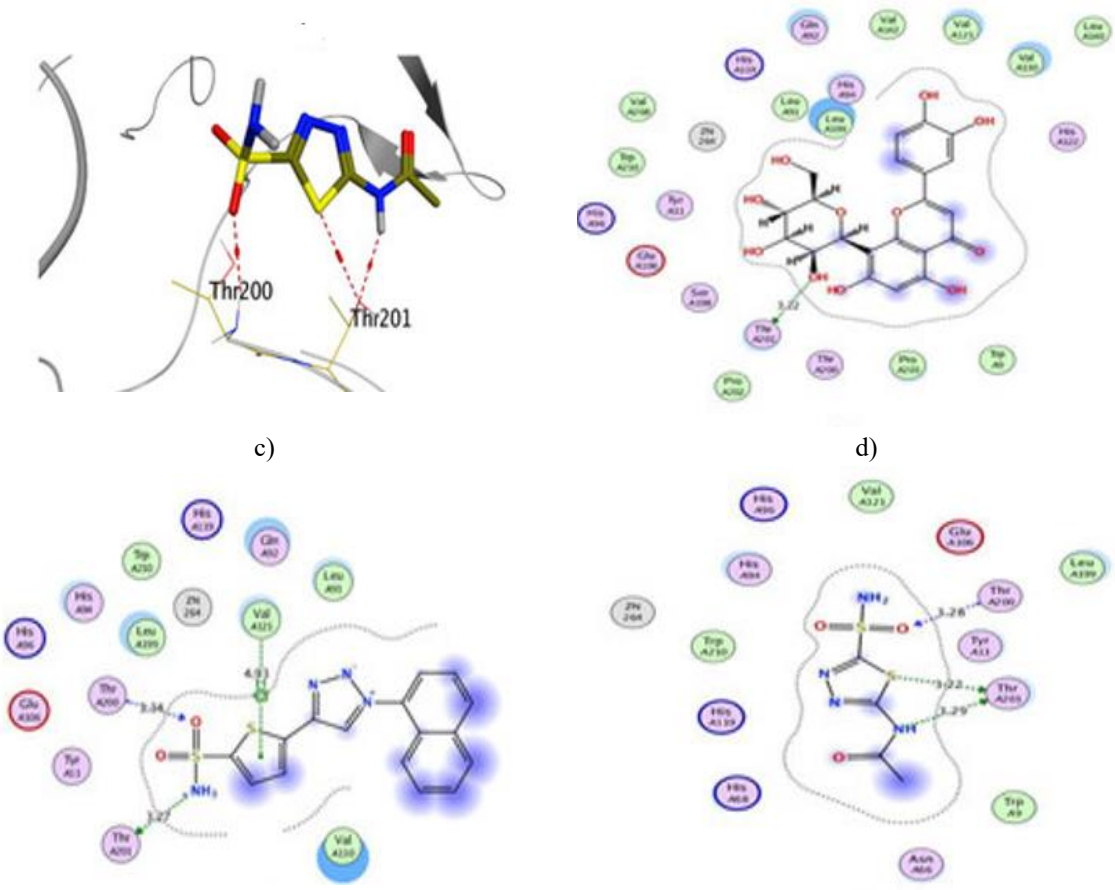

Figure 3. The 3D binding interactions of (a) compound 7, (b) the co-crystallized ligand, (c) the reference drug, and the 2D binding interactions of (d) compound 7, (e) the co-crystallized ligand, and (f) the reference drug at the CA IX.

Regarding the fatty acid synthase (FAS) biological target, compound (5) again showed the highest binding affinity among the series. The amino acids SER2340, TYR2462, and HIS2481 were identified as key players in FAS inhibition, based on their interactions with the co-crystallized ligand. It was thus observed that compound (5) could bind to FAS, yielding a binding energy of −6.82 Kcal/mol and an RMSD of 2.26 Å. In terms of binding details, the phenyl ring of compound (5) was involved in a pair of hydrogen bonds with SER2340 at distances of 2.97 and 3.02 Å. Concurrently, the benzopyran nucleus of compound (5) engaged PHE2370 and ILE2250 through pi-H interactions at distances of 4.53 and 3.8 Å, respectively. For the co-crystallized ligand, its aliphatic chain regions formed pi-H bonds with HIS2481 (4.42 Å) and TYR2462 (4.65 Å), while its carbonyl oxygen made a hydrogen bond to SER2340 at a 3.03 Å distance. In comparison, the phenyl ring system of the control drug ((-)-Epigallocatechin gallate) formed a pi-H interaction with HIS2481 at a distance of 3.92 Å, as displayed in **Figure 4**.

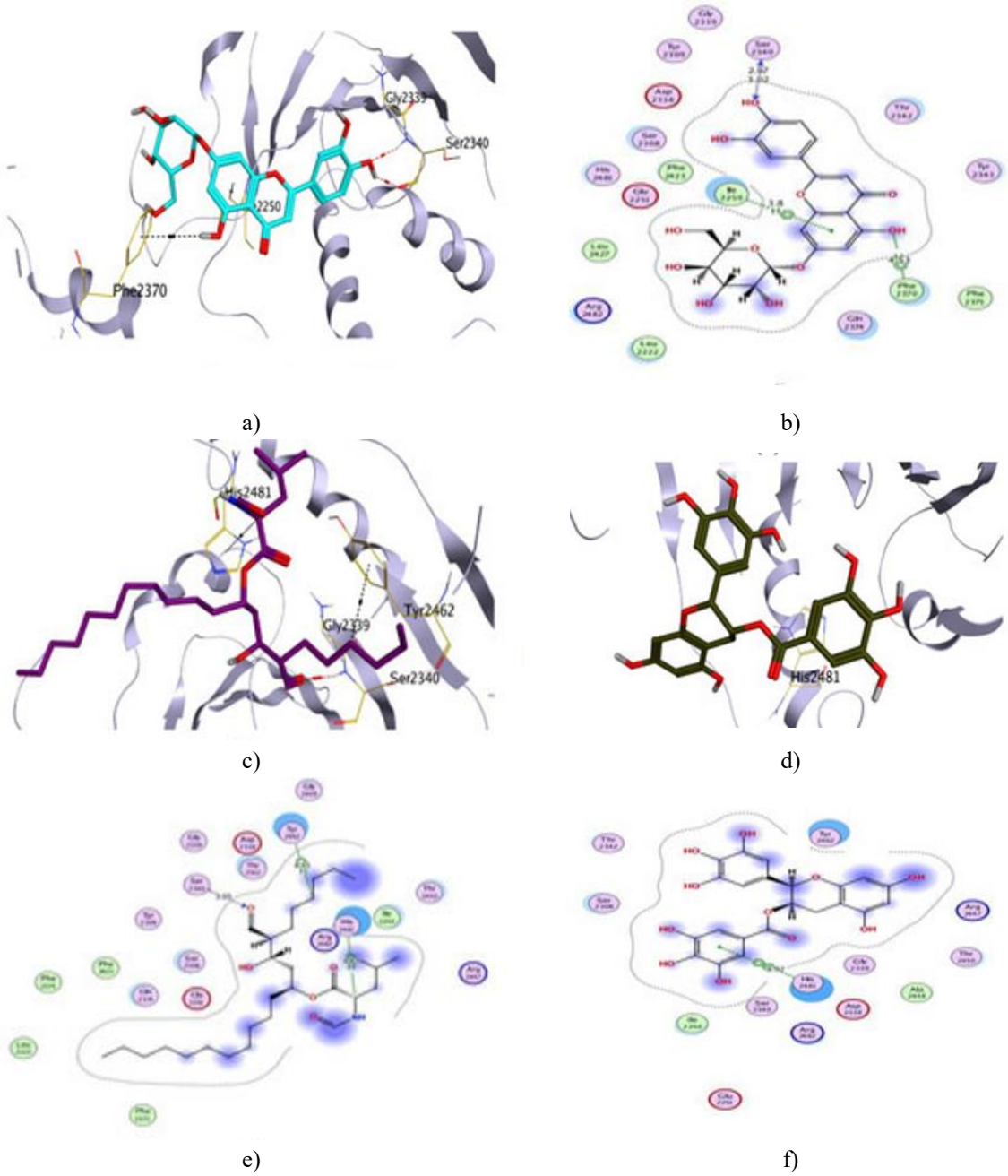

Figure 4. The 3D binding interactions of (a) compound 5, (b) the co-crystallized ligand, (c) the reference drug, and the 2D binding interactions of (d) compound 5, (e) the co-crystallized ligand, and (f) the reference drug at the FAS.

Turning attention to the Topoisomerase II-DNA complex (TOP II) as a biological target, it was noteworthy that compound (5) exhibited the greatest binding propensity within the entire panel of docked ligands. Prior studies have established that the principal binding loci of TOP II include the nucleotide bases ADE12, GUA13, CYT8, CYT11, and THY9, as well as the protein side chains ASP479, ARG503, GLN778, and MET782 [53]. In accordance with this, compound (5) was observed to coordinate with the TOP II complex, registering a binding free energy of −7.99 Kcal/mol and an RMSD value of 2.15 Å. To elaborate, the carbohydrate substituent of compound (5) forged hydrogen-bonding contacts with SER480 and DG at separations of 2.92 and 3.2 Å, respectively. Concurrently, its benzopyran ring system established a pi-H contact with DT at a 3.64 Å spacing, while a hydroxyl functionality decorating this same benzopyran moiety formed a hydrogen bond to ASP479 at a 2.69 Å distance. When examining the co-crystallized ligand, its sugar fragment participated in a pi-H interaction with DA and an H-bond with DG at respective distances of 3.75 and 3.37 Å. The dioxane unit within this co-crystallized ligand supplied additional H-bonds to GLN778 (2.94 Å) and MET782 (3.73 Å), and a hydroxyl

attached to its cyclohexyl moiety contributed an H-bond to ASP479 at 2.7 Å. For the comparator drug (Doxorubicin), its tetrahydrotetracene backbone mediated H-bonds with ASP479 (3.43 Å) and ARG503 (3.24 Å) in addition to a pi-H interaction with DG13 at 4.26 Å. A further H-bond linked a pyran-ring hydroxyl of Doxorubicin to LYS456 at 3.29 Å, as depicted in **Figure 5**.

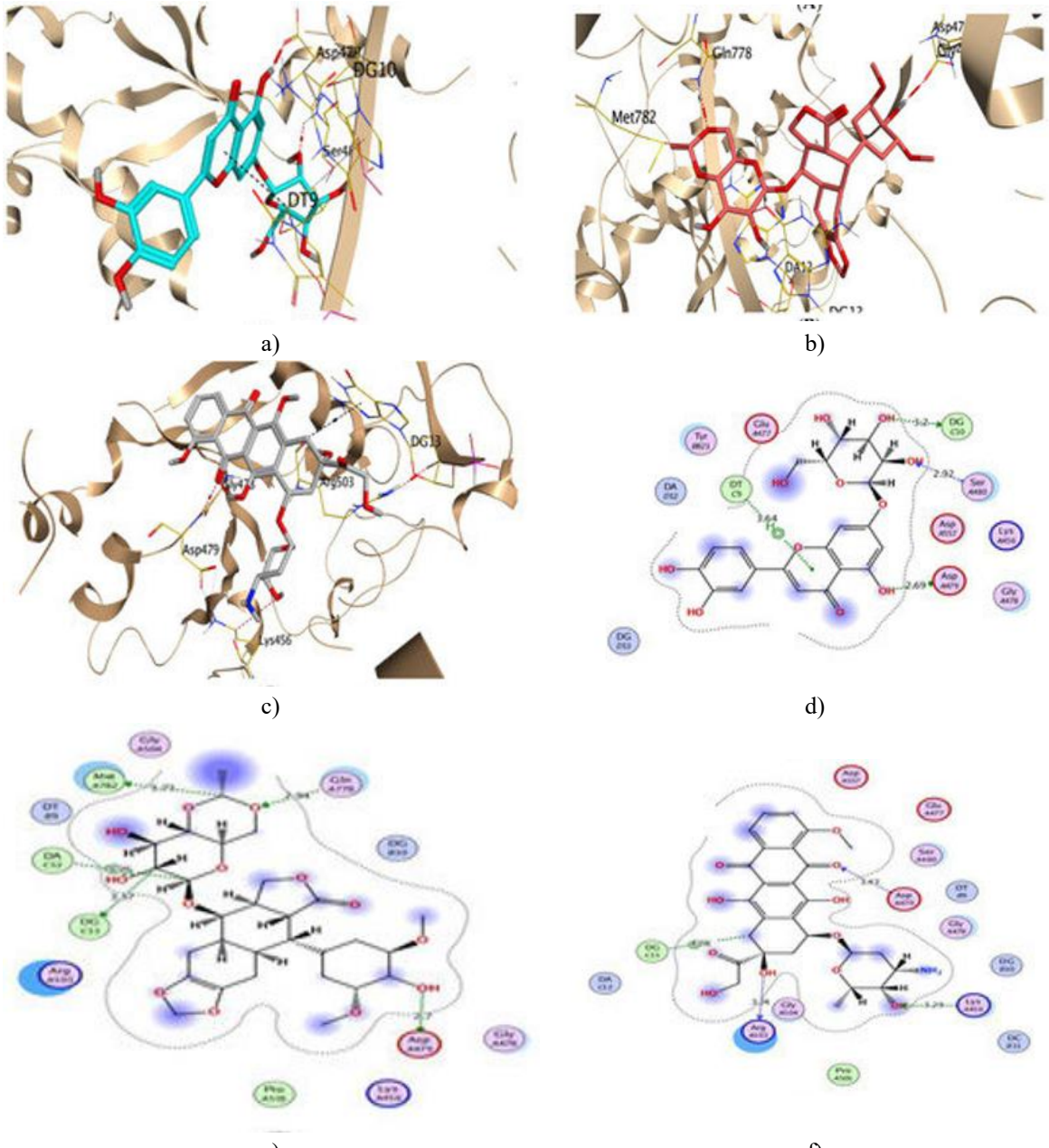

a) b) c) d) e) f)

Figure 5. The 3D binding interactions of (a) compound (5), (b) the co-crystallized ligand, (c) the reference drug, and the 2D binding interactions of (d) compound (5), (E) the co-crystallized ligand, and (f) the reference drug at the TOP II.

Prediction of physicochemical and pharmacokinetic properties

The submitted molecular structures were projected to exhibit suitable physicochemical and pharmacokinetic properties; the computed logPo/w values ranged from 1.0 to 2.89, coupled with strong aqueous solubility, as outlined in **Table 3** [30]. Satisfactory gastrointestinal uptake and oral bioavailability necessitate that a compound's physicochemical descriptors reside within prescribed limits [54]. The radar charts generated by the SwissADME web utility, shown in **Figure 6**, depict the oral bioavailability profiles of our target molecules. This graphical representation incorporates six axes corresponding to the six determinants of oral bioavailability: flexibility

(FLEX), lipophilicity (LIPO), size (SIZE), polarity (POLAR), solubility (INSOLU), and saturation (INSATU); the pink zone demarcates the ideal parameter space linked to a favorable oral bioavailability forecast [55]. As shown in **Figure 6**, the red polyline tracing Nepetanudoside C falls entirely within the pink region, suggesting strong oral bioavailability. Likewise, the red outlines symbolizing the remaining compounds are predominantly enclosed by the pink zone, suggesting acceptable oral bioavailability predictions. Beyond this, the SwissADME tool indicated that geniposide and nepetanudoside C adhere to Lipinski's rule, a pivotal drug-likeness filter, suggesting that these candidates may possess promising pharmacokinetic properties [56].

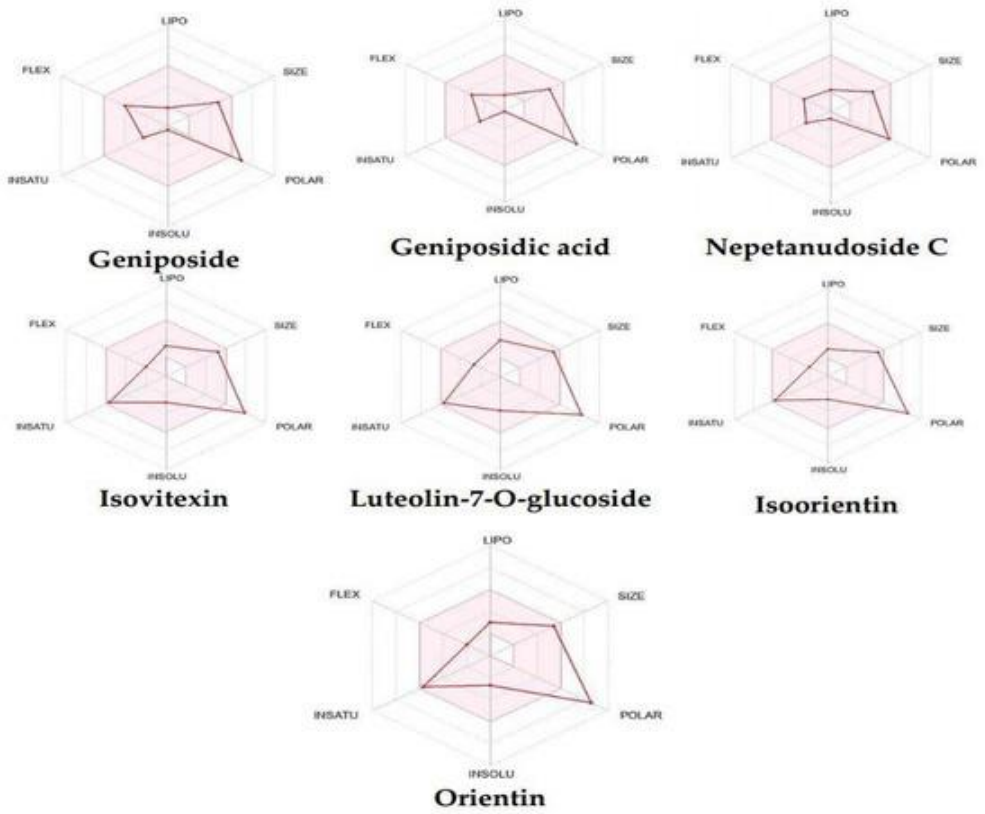

Figure 6. Radar charts for the prediction of oral bioavailability generated by the SwissADME web tool.

Table 3. ADMET profile of the target compounds.

Physicochemical Properties							
Parameter	**Orientin**	**Isoorientin**	**Luteolin-7-O-glucoside**	**Isovitexin**	**Nepetanudoside C**	**Geniposidic acid**	**Geniposide**
Molecular weight	448.10	448.10	448.10	432.11	342.13	374.12	388.14
LogP	1	1.6	1.99	1.97	1.22	1.31	2.89
Rotatable bonds	3	3	4	3	4	5	6
H-bond acceptors	11	11	11	10	8	10	10
H-bond donors	8	8	7	7	4	6	5
Molecular surface area (Å²)	201.28	201.28	190.28	181.05	125.68	166.14	155.14
Drug-Likeness evaluation							
Parameter	**Orientin**	**Isoorientin**	**Luteolin-7-O-glucoside**	**Isovitexin**	**Nepetanudoside C**	**Geniposidic Acid**	**Geniposide**

Lipinski rule violations	2	2	2	1	0	1	0
Ghose rule violations	1	1	0	0	1	1	1
Veber rule violations	1	1	1	1	0	1	1
Pharmacokinetic Properties							
Parameter	**Orientin**	**Isoorientin**	**Luteolin-7-O-glucoside**	**Isovitexin**	**Nepetanudoside C**	**Geniposidic acid**	**Geniposide**
GI absorption	Low	Low	Low	Low	High	Low	Low
BBB permeation	No	No	No	No	No	No	No
CYP1A2 inhibition	No	No	No	No	No	No	No
CYP2C19 inhibition	No	No	No	No	No	No	No
CYP2C9 inhibition	No	No	No	No	No	No	No
CYP2D6 inhibition	No	No	No	No	No	No	No
CYP3A4 inhibition	No	No	No	No	No	No	No

Conclusion

The study described herein culminated in the separation, structural identification, and spectroscopic characterization of seven phytoconstituents documented for the first time from the aerial organs of *P. frutescens* Hochst. Of particular note, the virtual screening component through molecular docking disclosed that Luteolin-7-O-glucoside (5) attained the most favorable binding energies among the analyzed set toward aromatase, fatty acid synthase, and the topoisomerase II-DNA complex, whereas Orientin (7) achieved the highest-ranked binding affinity toward carbonic anhydrase IX. These encouraging binding profiles were achieved by establishing robust hydrogen-bonding networks with catalytic-pocket residues and meaningful contacts with ancillary receptor-binding amino acids. The SwissADME online platform further projected that Luteolin-7-O-glucoside meets acceptable thresholds for pharmacokinetic performance and drug-likeness. On this basis, Luteolin-7-O-glucoside (5) and Orientin (7) merit recognition as lead scaffolds amenable to structural refinement aimed at crafting more powerful anticancer therapeutics. Research currently in progress involves synthesizing novel analogs and profiling the most active entities in vitro across multiple cell lines and enzymatic assay systems. In vivo experimentation using animal models is advised to advance these molecular candidates to the next stage of the drug discovery continuum.

Acknowledgments: None

Conflict of Interest: None

Financial Support: None

Ethics Statement: None

References

1. Kletter C, Kriechbaum M. *Tibetan Medicinal Plants*. Boca Raton (FL): CRC Press; 2001.
2. El-Hela AA, Hegazy MM, Bakr MSA, Abbass HS. Profiling of antiviral and antioxidant phytochemicals of *Pterocephalus frutescens* Hochist. using high-resolution ultra-performance liquid chromatography/quadrupole time-of-flight mass spectrometer. Pharmacogn Mag. 2020;16:592-9.

3. Guo C, Wu Y, Zhu Y, Wang Y, Tian L, Lu Y, et al. In vitro and in vivo antitumor effects of n-butanol extracts of *Pterocephalus hookeri* on Hep3B cancer cell. Evid Based Complement Alternat Med. 2015;2015:159132.
4. Fahem A, Ahmed A, Maha M, Soltan A, Hussein A, Zaki A. Anti-hepatotoxic effect of *Pterocephalus sanctus* growing in Egypt. JASRM. 2008;3:83-7.
5. Vahedi H, Nasrabadi M, Lari J, Halimi M. Volatile constituents and antimicrobial activities of *Pterocephalus canus*. J Med Plants Res. 2011;5:5646-8.
6. Wu YC, Guo CX, Zhu YZ, Li YM, Guo FJ, Zhu GF. Four new bis-iridoids isolated from the traditional Tibetan herb *Pterocephalus hookeri*. Fitoterapia. 2014;98:104-9.
7. Ahmed FA, Shahat AA. Flavonoid C-glycosides from *Pterocephalus sanctus* growing in Egypt. Nat Prod Commun. 2006;1:1934578X0600100605.
8. Gülcemal D, Masullo M, Alankuş-Çalışkan O, Karayıldırım T, Şenol SG, Piacente S, et al. Monoterpenoid glucoindole alkaloids and iridoids from *Pterocephalus pinardii*. Magn Reson Chem. 2010;48:239-43.
9. Gülcemal D, Bedir E, Karayıldırım T, Milena M, Piacente S, Şenol S, et al. Constituents of *Pterocephalus pinardii* Boiss. Planta Med. 2009;75:PJ103.
10. Li MY, Deng H, Zhao JM, Dai D, Tan XY. Peroxisome proliferator-activated receptor gamma ligands inhibit cell growth and induce apoptosis in human liver cancer BEL-7402 cells. World J Gastroenterol. 2003;9:1683-8.
11. Smith JA, Maloney DJ, Hecht SM, Lannigan DA. Structural basis for the activity of the RSK-specific inhibitor, SL0101. Bioorg Med Chem. 2007;15:5018-34.
12. Gordaliza M. Natural products as leads to anticancer drugs. Clin Transl Oncol. 2007;9:767-76.
13. Ren W, Qiao Z, Wang H, Zhu L, Zhang L. Flavonoids: Promising anticancer agents. Med Res Rev. 2003;23:519-34.
14. El-Hela AA, Hegazy MM, Abbass HS, Ahmed AH, Bakr MSA, Elkousy RH, et al. *Dinebra retroflexa* herbal phytotherapy: A simulation study based on bleomycin-induced pulmonary fibrosis retraction potential in Swiss albino rats. Medicina. 2022;58:1719.
15. Chumsri S, Howes T, Bao T, Sabnis G, Brodie A. Aromatase, aromatase inhibitors, and breast cancer. J Steroid Biochem Mol Biol. 2011;125:13-22.
16. Gu L, Saha ST, Thomas J, Kaur M. Targeting cellular cholesterol for anticancer therapy. FEBS J. 2019;286:4192-208.
17. Almeida CF, Teixeira N, Oliveira A, Augusto TV, Correia-da-Silva G, Ramos MJ, et al. Discovery of a multi-target compound for estrogen receptor-positive (ER+) breast cancer: Involvement of aromatase and ERs. Biochimie. 2021;181:65-76.
18. Sanderson JT, Hordijk J, Denison MS, Springsteel MF, Nantz MH, Berg MVD. Induction and inhibition of aromatase (CYP19) activity by natural and synthetic flavonoid compounds in H295R human adrenocortical carcinoma cells. Toxicol Sci. 2004;82:70-9.
19. Kuhajda FP, Pizer ES, Li JN, Mani NS, Frehywot GL, Townsend CA. Synthesis and antitumor activity of an inhibitor of fatty acid synthase. Proc Natl Acad Sci U S A. 2000;97:3450-4.
20. Fhu CW, Ali A. Fatty acid synthase: An emerging target in cancer. Molecules. 2020;25:3935.
21. Brusselmans K, Vrolix R, Verhoeven G, Swinnen JV. Induction of cancer cell apoptosis by flavonoids is associated with their ability to inhibit fatty acid synthase activity. J Biol Chem. 2005;280:5636-45.
22. Hegazy MM, Afifi WM, Metwaly AM, Radwan MM, Abd-Elraouf M, Mehany ABM, et al. Antitrypanosomal, antitopoisomerase-I, and cytotoxic biological evaluation of some African plants belonging to Crassulaceae; chemical profiling of extract using UHPLC/QTOF-MS/MS. Molecules. 2022;27:8809.
23. Bjornsti MA, Kaufmann SH. Topoisomerases and cancer chemotherapy: Recent advances and unanswered questions. F1000Res. 2019;8:1704.
24. Han S, Lim KS, Blackburn BJ, Yun J, Putnam CW, Bull DA, et al. The potential of topoisomerase inhibitor-based antibody-drug conjugates. Pharmaceutics. 2022;14:1707.
25. Okura A, Arakawa H, Oka H, Yoshinari T, Monden Y. Effect of genistein on topoisomerase activity and on the growth of [VAL 12]Ha-ras-transformed NIH 3T3 cells. Biochem Biophys Res Commun. 1988;157:183-9.
26. Hevener K, Verstak TA, Lutat KE, Riggsbee DL, Mooney JW. Recent developments in topoisomerase-targeted cancer chemotherapy. Acta Pharm Sin B. 2018;8:844-61.

27. Pastorekova S, Gillies RJ. The role of carbonic anhydrase IX in cancer development: Links to hypoxia, acidosis, and beyond. Cancer Metastasis Rev. 2019;38:65-77.
28. Saghafi T, Taheri RA, Parkkila S, Emameh RZ. Phytochemicals as modulators of long non-coding RNAs and inhibitors of cancer-related carbonic anhydrases. Int J Mol Sci. 2019;20:2939.
29. McDonald PC, Chafe SC, Supuran CT, Dedhar S. Cancer therapeutic targeting of hypoxia induced carbonic anhydrase IX: From bench to bedside. Cancers (Basel). 2022;14:3297.
30. Daina A, Michielin O, Zoete V. SwissADME: A free web tool to evaluate pharmacokinetics, drug-likeness and medicinal chemistry friendliness of small molecules. Sci Rep. 2017;7:42717.
31. Elmaaty AA, Darwish KM, Khattab M, Elhady SS, Salah M, Hamed MI, et al. In a search for potential drug candidates for combating COVID-19: Computational study revealed salvianolic acid B as a potential therapeutic targeting 3CLpro and spike proteins. J Biomol Struct Dyn. 2021;40:8866-93.
32. Elmaaty AA, Alnajjar R, Hamed MI, Khattab M, Khalifa MM, Al-Karmalawy AA. Revisiting activity of some glucocorticoids as a potential inhibitor of SARS-CoV-2 main protease: Theoretical study. RSC Adv. 2021;11:10027-42.
33. Elmaaty AA, Hamed MI, Ismail MI, Elkaeed EB, Abulkhair HS, Khattab M, et al. Computational insights on the potential of some NSAIDs for treating COVID-19: Priority set and lead optimization. Molecules. 2021;26:3772.
34. Hamed MI, Darwish KM, Soltane R, Chrouda A, Mostafa A, Shama NMA, et al. β-Blockers bearing hydroxyethylamine and hydroxyethylene as potential SARS-CoV-2 Mpro inhibitors: Rational based design, in silico, in vitro, and SAR studies for lead optimization. RSC Adv. 2021;11:35536-58.
35. Elmaaty AA, Darwish KM, Chrouda A, Boseila AA, Tantawy MA, Elhady SS, et al. In silico and in vitro studies for benzimidazole anthelmintics repurposing as VEGFR-2 antagonists: Novel mebendazole-loaded mixed micelles with enhanced dissolution and anticancer activity. ACS Omega. 2022;7:875-99.
36. Elebeedy D, Badawy I, Elmaaty AA, Saleh MM, Kandeil A, Ghanem A, et al. In vitro and computational insights revealing the potential inhibitory effect of tanshinone IIA against influenza A virus. Comput Biol Med. 2021;141:105149.
37. Hammoud MM, Nageeb AS, Morsi MA, Gomaa EA, Elmaaty AA, Al-Karmalawy AA. Design, synthesis, biological evaluation, and SAR studies of novel cyclopentaquinoline derivatives as DNA intercalators, topoisomerase II inhibitors, and apoptotic inducers. New J Chem. 2022;46:11422-36.
38. Hammoud MM, Elmaaty AA, Nafie MS, Abdel-Motaal M, Mohamed NS, Tantawy MA, et al. Design and synthesis of novel benzoazoninone derivatives as potential CBSIs and apoptotic inducers: In vitro, in vivo, molecular docking, molecular dynamics, and SAR studies. Bioorg Chem. 2022;127:105995.
39. Ghosh D, Egbuta C, Lo J. Testosterone complex and non-steroidal ligands of human aromatase. J Steroid Biochem Mol Biol. 2018;181:11-9.
40. Leitans J, Kazaks A, Balode A, Ivanova J, Zalubovskis R, Supuran CT, et al. Efficient expression and crystallization system of cancer-associated carbonic anhydrase isoform IX. J Med Chem. 2015;58:9004-9.
41. Pemble CW, Johnson LC, Kridel SJ, Lowther WT. Crystal structure of the thioesterase domain of human fatty acid synthase inhibited by orlistat. Nat Struct Mol Biol. 2007;14:704-9.
42. Wu CC, Li TK, Farh L, Lin LY, Lin TS, Yu YJ, et al. Structural basis of type II topoisomerase inhibition by the anticancer drug etoposide. Science. 2011;333:459-62.
43. Güvenalp Z, Kilic N, Kazaz C, Kaya Y, Demirezer LÖ. Chemical constituents of *Galium tortumense*. Turk J Chem. 2006;30:515-23.
44. Takeda Y, Morimoto Y, Matsumoto T, Honda G, Tabata M, Fujita T, et al. Nepetanudoside, an iridoid glucoside with an unusual stereostructure from *Nepeta nuda* ssp. *albiflora*. J Nat Prod. 1995;58:1217-21.
45. Huang D, Guo W, Gao J, Chen J, Olatunji JO. *Clinacanthus nutans* (Burm. f.) Lindau ethanol extract inhibits hepatoma in mice through upregulation of the immune response. Molecules. 2015;20:17405-28.
46. de Oliveira D, Siqueira EP, Nunes YRF, Cota BB. Flavonoids from leaves of *Mauritia flexuosa*. Rev Bras Farmacogn. 2013;23:614-20.
47. Chiruvella KK, Mohammed A, Dampuri G, Ghanta RG, Raghavan SC. Phytochemical and antimicrobial studies of methyl angolensate and luteolin-7-O-glucoside isolated from callus cultures of *Soymida febrifuga*. Int J Green Pharm. 2007;3:269-78.

48. El-Demerdash A, Al-Karmalawy AA, Abdel-Aziz TM, Elhady SS, Darwish KM, Hassan AHE. Investigating the structure-activity relationship of marine natural polyketides as promising SARS-CoV-2 main protease inhibitors. RSC Adv. 2021;11:31339-63.
49. Elebeedy D, Elkhatib WF, Kandeil A, Ghanem A, Kutkat O, Alnajjar R, et al. Anti-SARS-CoV-2 activities of tanshinone IIA, carnosic acid, rosmarinic acid, salvianolic acid, baicalein, and glycyrrhetinic acid between computational and in vitro insights. RSC Adv. 2021;11:29267-86.
50. Khattab M, Al-Karmalawy AA. Computational repurposing of benzimidazole anthelmintic drugs as potential colchicine binding site inhibitors. Future Med Chem. 2021;13:1623-38.
51. Ghanem A, Al-Karmalawy AA, El Maksoud AIA, Hanafy SM, Emara HA, Saleh RM, et al. *Rumex vesicarius* L. extract improves the efficacy of doxorubicin in triple-negative breast cancer through inhibiting Bcl2, mTOR, JNK1 and augmenting p21 expression. Inform Med Unlocked. 2022;29:100869.
52. Asmari M, Waqas M, Ibrahim AE, Halim SA, Khan A, Al-Harrasi A, et al. Microscale thermophoresis and molecular modelling to explore the chelating drug transportation in the milk to infant. Molecules. 2022;27:4604.
53. El-Naggar AM, Abou-El-Regal MM, El-Metwally SA, Sherbiny FF, Eissa IH. Synthesis, characterization and molecular docking studies of thiouracil derivatives as potent thymidylate synthase inhibitors and potential anticancer agents. Mol Divers. 2017;21:967-83.
54. Gomaa E, El Deeb S, Ibrahim AE, Faisal MM. Bimodal release two-in-one clonazepam matrix lozenge tablets for managing anxiety-related disorders: Formulation, optimization and in vivo evaluation. Sci Pharm. 2022;90:43.
55. Daina A, Michielin O, Zoete V. iLOGP: A simple, robust, and efficient description of n-octanol/water partition coefficient for drug design using the GB/SA approach. J Chem Inf Model. 2014;54:3284-301.
56. Lipinski CA, Lombardo F, Dominy BW, Feeney PJ. Experimental and computational approaches to estimate solubility and permeability in drug discovery and development settings. Adv Drug Deliv Rev. 2012;64:4-17.